Proceedings of the ASME 2018 International Design Engineering Technical Conferences and Computers and Information in Engineering Conference IDETC/CIE 2018 August 26-29, 2018, Quebec City, Quebec, Canada

DETC2018-85543

A MEMS THRESHOLD ACCELERATION SWITCH POWERED BY A TRIBOELECTRIC GENERATOR

Mark Pallay
Mechanical Engineering Department
Binghamton University
Binghamton, New York, 13902
mpallay1@binghamton.edu

Alwathiqbellah I Ibrahim
Mechanical Engineering Department
Binghamton University
Binghamton, New York, 13902
aibrahi4@binghamton.edu

Shahrzad Towfighian*
Mechanical Engineering Department
Binghamton University
Binghamton, New York, 13902
stowfigh@binghamton.edu

ABSTRACT

In this paper a novel electrostatic MEMS combined shock sensor and normally-closed switch is presented. The switch uses combined attractive and repulsive forcing to toggle a cantilever beam to and from the pulled-in position. The attractive force is generated through a parallel plate electrode configuration and induces pull-in. The repulsive force is generated through electrostatic levitation from a third electrode and serves to pull the beam out of its pulled-in position. A triboelectric transducer converts impact energy to electrical energy to provide voltage for the third electrode, which temporarily opens the switch if enough impact energy is supplied. Triboelectricity addresses the high voltage requirement for electrostatic levitation. The multi-electrode sensor also addresses the low current output from the generator because it acts as an open circuit between the parallel plate and levitation electrodes. A theoretical model of the switch is derived to analyze stability and the dynamic response of the cantilever. Threshold voltages to pull-in and release the beam through repulsive forcing is calculated. Output voltage plots from a prototype generator under a single impact are applied to the sensor-switch model to demonstrate the working principle of the sensor-switch is feasible.

*Address all correspondence to this author.

INTRODUCTION

With increasing demand for high performance and technologically advanced electronic devices, more efficient and reliable sensors are needed to achieve the performance that has come to be expected of new technology. Sensors play a vital role in these devices by enabling them to interact with and acquire information from the user, their environment, and from themselves. Because of the demand for fast, simple, and energy efficient electronic devices, microelectromechanical systems (MEMS) are often used as sensors for their fast response time, low bulk fabrication costs, and low power consumption [1].

MEMS have a tremendous range of applications and can be used as sensors [2–4], switches [5, 6], energy harvesters [7–11], signal filters [12–15], etc, or for multiple applications at once [16, 17] (e.g. a sensor-switch). Many of these devices use electrostatic actuation because it can be easily fabricated, consumes minimal power, and can be integrated in electronic circuits without much difficulty [1]. Traditional electrostatic actuation utilizes a parallel plate capacitor configuration with electrostatic forces pulling a movable electrode (typically a beam or plate) towards a fixed one. This can cause the electrodes to collapse if the voltage potential between them is high enough (pull-in). For switches, this is desirable because it closes a circuit between the electrodes if the contacting faces are conductive. Therefore a MEMS switch can be toggled to closed by applying the pull-in voltage between the electrodes. While pull-in is necessary for switches, it is usually undesirable for sensors, which in many

cases need the ability to move freely.

Some effort has been made to eliminate the pull-in instability by exploiting electrostatic levitation [18–30]. This creates an effectively repulsive force between the two electrodes instead of an attractive one. Lee and Cho [18] first applied a similar concept to a MEMS device in 2001 where they demonstrated that two grounded electrodes would be pulled away from each other when in close proximity to a charged electrode on their side. He and Ben-Mrad flipped this design on its side to create out of plane actuation [21]. This configuration, shown in Figure 1, has a beam placed above a fixed electrode, both of which are grounded. Two charged electrodes are placed on either side of the fixed electrode and generate a net electrostatic force on the beam away from the substrate. Because the electrostatic force is generated through the fringe field, a very large voltage is needed to actuate the beam. This requirement of high voltage can easily be satisfied by connecting the actuator to a triboelectric generator.

Triboelectricity has been investigated in recent years as a possible transduction mechanism for converting mechanical energy to electrical energy because of its high energy conversion efficiency and large voltage output [31–39]. Triboelectric charging occurs when two materials with different affinities to gain or lose electrons are brought into contact with each other. Electrons are passed from one material to another at the contact area to equalize the potential at the interface. These materials retain their charge even after the materials have been separated. Despite its large voltage, the current produced is on the order of nanoamps. However, the repulsive force electrode configuration from [21] acts as a completely open circuit between the side electrodes and beam/center electrode, requiring no current. This means the high output voltage of a tribolelectric generator can be exploited for this purpose without the downside of a low power output.

The working principle of a triboelectric generator (TEG) is based on coupling between triboelectrification and electrostatic induction [40]. A 3D model of the generator can be seen in Figure 2. The TEG consists of two aluminum electrodes (one fixed, one free) and a PDMS insulator. The PDMS is mounted on the fixed electrode with the exposed face machined to increase surface area. The free electrode is also machined on one side with a reverse pattern and mounted above the PDMS with a set of springs or a clamped-clamped beam. When the generator receives an impact, the free electrode comes into contact with the PDMS and triboelectric charges are created. After the impact, the layers separate because of the springs and a potential difference is generated between the two electrodes. If the two electrodes are connected, the current will be induced through the wire to equalize the voltage potential. If the electrodes are disconnected, the PDMS retain its triboelectric charges, which allows the electrodes to stay charged for a short period of time, such as in the case of Figure 2.

In this paper a threshold shock sensor-switch is introduced. The sensor consists of a triboelectric generator connected to a

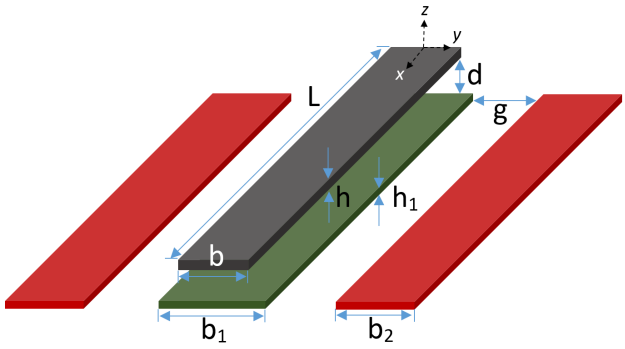

FIGURE 1. REPULSIVE FORCE ELECTRODE CONFIGURATION WITH CANTILEVER BEAM (BLACK), FIXED MIDDLE ELECTRODE (GREEN) AND FIXED SIDE ELECTRODES (RED). THE SIDE ELECTRODES ARE CONNECTED TOGETHER AND TREATED AS A SINGLE, THIRD ELECTRODE.

MEMS cantilever with a repulsive-force electrode configuration (Figure 1). A small bias voltage is applied between the beam and center electrode to initiate pull-in (Figure 2a). The generator is connected between the side and center electrodes and creates a large voltage potential between them when the generator receives an impact. The amount of voltage the generator produces is a function of the impact force magnitude, with a larger impact generating more voltage. This creates a large repulsive force that pulls the beam off of the substrate and opens the switch if the impact force is large enough (Figure 2b). Dimples are placed on the underside of the beam to reduce contact forces and prevent the beam from sticking to the substrate. Over the course of a few minutes the charge on the generator electrodes decays, which reduces the repulsive force until the switch pulls back in and closes itself. The sensor-switch can be designed such that when the impact force passes a threshold level, the switch is triggered and the beam is released from its pulled-in position.

The contribution of this work is to demonstrate the feasibility of powering a repulsive-force MEMS switch with a triboelectric generator that produces voltage from an impact to create a combined sensor-switch system. The repulsive-force electrode configuration allows for a very large dynamic range and can be exploited to eliminate the pull-in instability in electrostatic sensors. The triboelectric generator is capable of overcoming the large threshold voltage to actuate the beam via the electrostatic fringe field, and the multi-electrode repulsive-force sensor allows the generator to remain completely open circuit, eliminating the issue with low power output. This opens the possibility for a wide range of novel sensors with increased performance and functionality.

The organization of this paper is as follows: The next section outlines the formulation of the governing equation of motion for

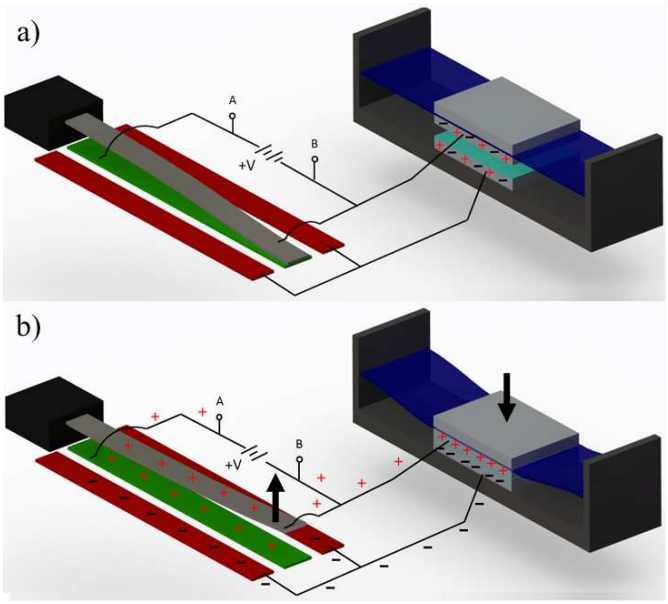

FIGURE 2. LAYOUT OF THE IMPACT SENSOR. TOP SHOWS SENSOR IN THE INITIAL CLOSE STATE PRIOR TO IMPACT. BOTTOM SHOWS SENSOR DURING IMPACT AS THE SWITCH IS OPENED.

the cantilever. Then the switch is characterized by calculating the threshold voltages needed to initial pull-in and release the beam. Next, voltage curves are experimentally extracted from a prototype generator and applied to the model to simulate the beam response. Lastly, our conclusions and future work are discussed in the final section.

THEORETICAL MODEL

The beam is linear-elastic polysilicon with dimensions and material properties given in Table 1. The beam is modeled using Euler-Bernoulli beam theory with geometric nonlinearities ignored.

$$\rho A \frac{\partial^2 \hat{w}}{\partial \hat{t}^2} + \hat{c} \frac{\partial \hat{w}}{\partial \hat{t}} + EI \frac{\partial^4 \hat{w}}{\partial \hat{x}^4} + \hat{f}_e(\hat{w}) = 0 \qquad (1)$$

In Equation (1), $\hat{w}$ is the transverse beam displacement, I is the moment of inertia, and $\hat{f}_e$ is the electrostatic force. The electrostatic force is calculated numerically with an FEA simulation in COMSOL, and a 9th order polynomial is fit to the data. Because the bias voltage between the cantilever and center electrodes remains constant, the electrostatic force will not scale with the square of the generator voltage. A new simulation and polynomial fit must be performed for a different generator voltage

TABLE 1. BEAM GEOMETRY AND MATERIAL PROPERTIES

Parameter	Symbol	Value
Cantilever Length (μm)	L	500
Beam Width (μm)	b	10
Beam Thickness (μm)	h	2
Beam-Electrode Gap (μm)	d	2
Electrode Gap (μm)	g	5
Electrode Width 1 (μm)	b_1	32
Electrode Width 2 (μm)	b_2	28
Electrode Thickness (μm)	h_1	0.5
Elastic Modulus (GPa)	E	158
Density ($^{kg}/_{m^3}$)	ρ	2330
Poisson's Ratio	ν	0.22

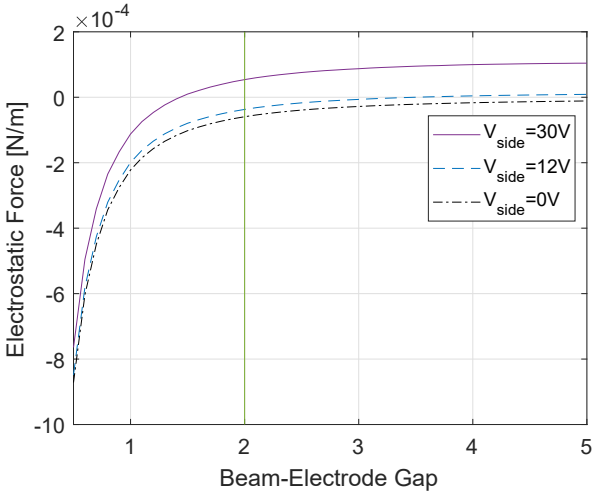

FIGURE 3. ELECTROSTATIC FORCE AS THE GAP BETWEEN ELECTRODES (d) VARIES AT A 2.2 V_{bias} AND 0, 12, AND 30 V_{side}. THE GREEN LINE INDICATES THE REST POSITION OF THE BEAM. THE RESULTS ARE OBTAINED FROM COMSOL SIMULATIONS

level. This means the polynomial coefficients are functions of the generator voltage, which is continually changing in time. The electrostatic force at 2.2 V_{bias} and several side voltages is shown in Figure 3.

Equation (1) is non-dimensionalized using the substitutions shown in Table 2, which gives the non-dimensional equation of

TABLE 2. NONDIMENSIONAL SUBSTITUTIONS

Parameter	Substitution
x-direction position	$x = \hat{x}/L$
z-direction position	$w = \hat{w}/h$
Time	$t = \hat{t}/T$
Damping	$c^* = \hat{c}L^4/EIT$
Time Constant	$T = \sqrt{\rho AL^4/EI}$
Force Constant	$r_1 = L^4/EIh$

motion as

$$\frac{\partial^2 w}{\partial t^2} + c^* \frac{\partial w}{\partial t} + \frac{\partial^4 w}{\partial x^4} + r_1 \sum_{j=0}^{9} p_j h^j w^j = 0 \tag{2}$$

where p_j are coefficients from the 9th order polynomial forcing fit, and are functions of the generator and bias voltages. Equation (2) is then reduced into a set of coupled ordinary differential equations (ODE) through Galerkin's method. First, separation of variables is performed on Equation (2), with the beam response approximated as

$$w(x,t) \approx \sum_{i=1}^{n} q_i(t)\phi_i(x) \tag{3}$$

where $\phi_i(x)$ are the mode shapes of the beam, $q_i(t)$ are the time dependent generalized coordinates, and n is the number of degrees of freedom (DOF). The effect of the electrostatic force on the mode shapes of the beam is neglected and thus the mode shapes for a cantilever micro-beam are given in Equation (4).

$$\phi_i(x) = \cosh(\alpha_i x) - \cos(\alpha_i x) - \sigma_i(\sinh(\alpha_i x) - \sin(\alpha_i x)) \tag{4}$$

where α_i^2 are the non-dimensional natural frequencies, and σ_i are constants that depend on the boundary conditions and mode. α_i and σ_i for the first three modes are obtained from [41].

Once the mode shapes are known, Equation (3) is plugged into Equation (2), which yields a coupled set of n ODE's for q_i.

$$\sum_{i=1}^{n}\left(\phi_i \frac{\partial^2 q_i}{\partial t^2} + c^*\phi_i \frac{\partial q_i}{\partial t} + \frac{\partial^4 \phi_i}{\partial x^4} q_i\right) + r_1 \sum_{j=0}^{9} p_j h^j \left(\sum_{i=0}^{n} q_i \phi_i\right)^j = 0 \tag{5}$$

To decouple the linear terms, Equation (5) is multiplied by ϕ_k and integrated over the length of the beam, resulting in,

$$m_i\ddot{q}_i + c_i\dot{q}_i + k_i q_i + r_1 \sum_{j=0}^{9} p_j h^j \int_0^1 \phi_k \left(\sum_{i=0}^{n} \phi_i q_i\right)^j dx = 0 \tag{6}$$

where nonlinear terms remain coupled and,

$$m_i = \int_0^1 \phi_i^2 dx \quad k_i = \alpha_1^4 m_i \quad c_i = c^* m_i \tag{7}$$

For a one mode approximation, Equation (6) becomes,

$$m_1\ddot{q}_1 + c_1\dot{q}_1 + k_1 q_1 + \sum_{j=0}^{9} f_j q_1^j = 0 \tag{8}$$

where

$$f_j = r_1 p_j h^j \int_0^1 \phi_1^{j+1} dx \tag{9}$$

A one mode model is used because one DOF is a very good approximation of the system, as verified in our previous experiment [28].

The damping coefficient is estimated using the quality factor, Q, and natural frequency, α_1^2.

$$c = \frac{\alpha_1^2}{Q} \tag{10}$$

The quality factor is assumed to be 70. Once all terms are defined, Equation (8) can be solved.

SWITCH CHARACTERIZATION

First, the pull-in voltage for the cantilever is calculated. This is the minimum required voltage for the switch to start in the closed state. Since the cantilever and center electrode act as a simple parallel plate actuator, the pull-in voltage can be calculated with the relationship shown in Equation (11).

$$V_{pull} = \sqrt{\frac{8k_1 d^3}{27\varepsilon A}} \tag{11}$$

where ε is the permittivity of air and A is the area of the underside of the beam. From Equation (11), the pull-in voltage should be approximately 1.9 V. Therefore 2.2 V (V_{bias}) is applied between the beam and center electrode so that the starting position of the switch is in the closed state. A voltage slightly higher than the pull-in voltage is necessary for the switch to stay closed because the dimples (0.75 μm long) do not allow the beam to travel the entire 2 μm gap. If the voltage is too low the beam will start to pull-in, but the force will be too weak to hold it in the pulled in position of -1.25 μm.

Next, the threshold generator voltage to open the switch when given an initial bias of 2.2 V is calculated. This can be estimated by calculating the potential energy and phase portrait. If the voltage is too low the beam should have an unstable trajectory in the phase plane. However, when the voltage exceeds a threshold it becomes stable and wants to settle to an equilibrium position somewhere above the substrate. The phase portrait will then show a periodic orbit about the equilibrium point.

To calculate the potential energy, Equation (8) is integrated. The damping has a small effect on the stability and is set to zero. This yields,

$$m_1 \frac{\dot{q_1}^2}{2} + k_1 \frac{q_1^2}{2} + \sum_{j=0}^{9} \frac{f_j}{j+1} q_1^{j+1} = H \tag{12}$$

In Equation (12) the first term is the kinetic energy, while the second two terms are the potential energy. H is the total energy of the system, which can be varied to view various trajectories in the phase portrait. Figure 4 shows the potential energy for the case of $V_{bias} = 2.2\ V$ and $V_{side} = 0V$, showing the system will pull in at this voltage.

To calculate the phase portrait, Equation (12) is rearranged to solve for $\dot{q_1}^2$, which is a pair of nonlinear function of q_1. The separatrix can be calculated by setting H to be the potential energy (V) at a local peak (if one exists). For the case of Figure 4, no such peak exists and the system remains unstable everywhere. Figure 5 shows the phase plane trajectory of the beam starting at rest for a bias voltage of 2.2 V.

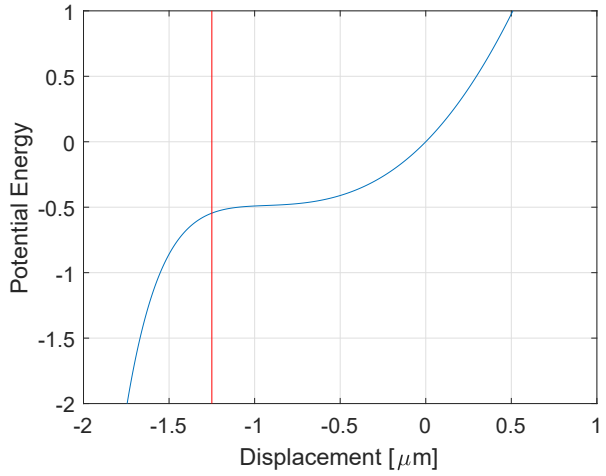

FIGURE 4. POTENTIAL ENERGY OF THE BEAM AS A FUNCTION OF TIP DISPLACEMENT AT $V_{bias} = 2.2\ V$ AND $V_{side} = 0V$. THE RED LINE INDICATES THE SMALLEST POSSIBLE GAP BECAUSE OF THE DIMPLES.

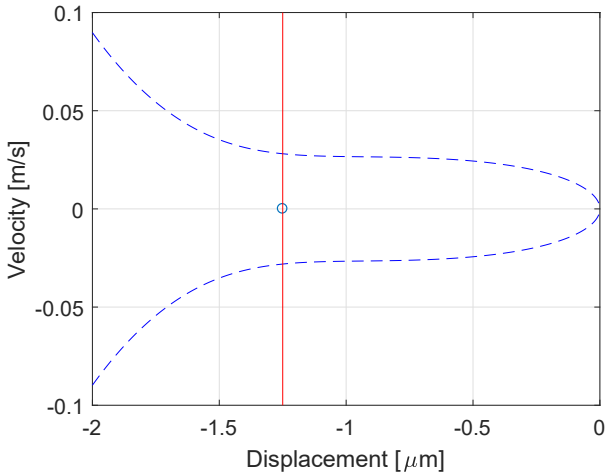

FIGURE 5. PHASE PORTRAIT AT $V_{bias} = 2.2\ V$ AND $V_{side} = 0V$. THE RED LINE INDICATES THE SMALLEST POSSIBLE GAP. THE MARKER SHOWS THE PULLED IN POSITION OF THE BEAM AT -1.25 μm AND ZERO VELOCITY

Next, the side voltage is gradually increased until the system becomes stable again. This occurs when the pulled-in position of the beam (indicated in the phase portrait by the intersection of the red line and zero velocity axis) moves inside of a closed loop in the phase portrait. A loop in the phase portrait occurs when a local minimum appears in the potential energy plot. If the side electrode voltage is increased past a threshold, the potential

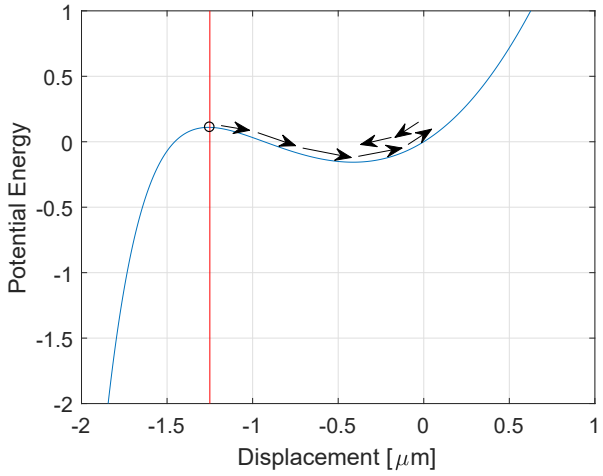

FIGURE 6. POTENTIAL ENERGY AT $V_{bias} = 2.2\ V$ AND $V_{side} = 12V$. THE RED LINE INDICATES THE SMALLEST POSSIBLE GAP. THE PULLED IN POSITION IS THE INTERSECTION OF THE RED AND BLUE LINE. THE ARROWS SHOW THE BEAM SETTLING TO ITS NEW EQUILIBRIUM POSITION.

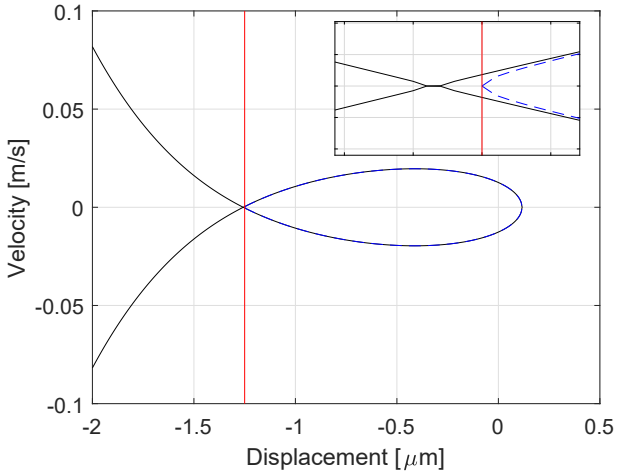

FIGURE 7. PHASE PORTRAIT AT $V_{bias} = 2.2\ V$ AND $V_{side} = 12V$. THE INLET SHOWS A ZOOMED IN PICTURE OF THE INTERSETION AT ZERO VELOCITY AND -1.25 μm.

well will grow large enough to allow the beam to oscillate in a stable orbit and the beam will release. Figures 6 and 7 show the potential energy and phase portrait respectively when the side electrode voltage is increased to 12 V.

As can be seen in the phase portrait (Figure 7), at side voltage of 12 V, the pulled-in position of the beam exists inside a closed loop indicating the beam is now stable. This means,

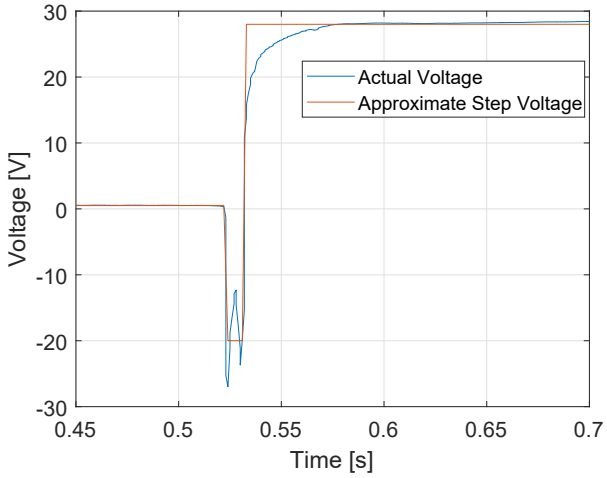

FIGURE 8. OPEN CIRCUIT GENERATOR VOLTAGE RESULTING FROM A SINGLE LIGHT IMPACT. THE VOLTAGE IS MEASURED WITH A KEITHLEY 6514 ELECTROMETER. THE VOLTAGE OUTPUT CAN BE ESTIMATED AS A SERIES OF STEP INPUTS.

neglecting stiction forces, only 12 V is necessary to open the switch. Contact forces holding the beam in the pulled-in position will inevitably increase this threshold, however it can be difficult to estimate theoretically and thus its influence will be determined through an experiment. The tribolelectric generator is capable of producing voltages over an order of magnitude above the calculated threshold. This allows the bias voltage to be increased significantly to tune the sensitivity of the sensor. It also opens the possibility of miniaturizing the generator to the millimeter or even smaller scale, which is very attractive for MEMS sensors. Both threshold voltages to close and open the switch have been verified through integration of Equation (8).

RESULTS

Next, the generator output was experimentally extracted using a prototype triboelectric generator from [40]. The generator was struck with a 1 lb weight to see the open circuit voltage produced from a single impact. Figures 8 and 9 show the voltage plots for two separate impact tests.

In Figures 8 and 9 the voltage responds in two steps during the impact. For the smaller impact (Figure 8) the first step is a negative voltage, while for the larger impact (Figure 9) the first step is a positive voltage. The reason for this difference is still under investigation but does not significantly affect the operation of the device. The delay between steps is relatively short at 10 ms and 25 ms respectively. However, the beam response period is less than 0.1 ms and therefore the short delay can not be ignored.

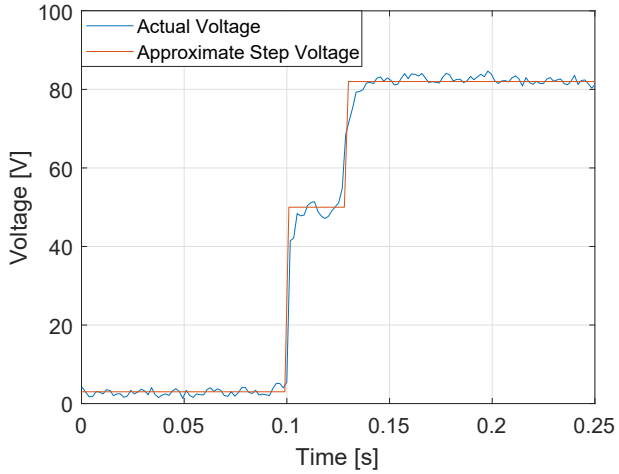

FIGURE 9. OPEN CIRCUIT GENERATOR VOLTAGE RESULTING FROM A SINGLE HARDER IMPACT. THE HARDER IMPACT RESULTS IN A HIGHER OUTPUT VOLTAGE. THE VOLTAGE IS MEASURED WITH A KEITHLEY 6514 ELECTROMETER. THE VOLTAGE OUTPUT CAN BE ESTIMATED AS A SERIES OF STEP INPUTS.

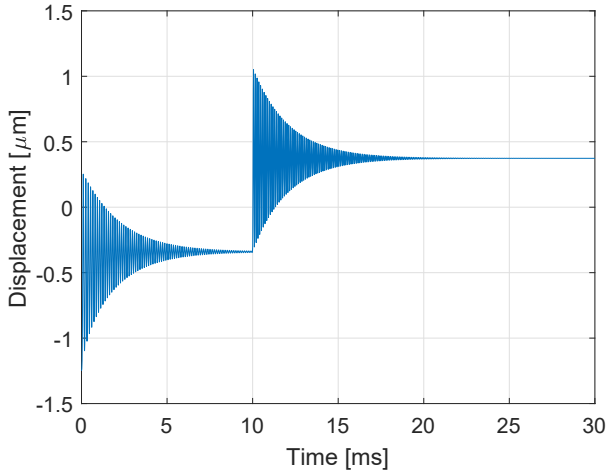

FIGURE 10. BEAM TIP DISPLACEMENT FOR A SIDE VOLTAGE CORRESPONDING TO THE STEP VOLTAGE SHOWN IN FIGURE 8. THE FIRST VOLTAGE STEP IS AT TIME ZERO AND THE SECOND VOLTAGE STEP IS AFTER 10 ms. THE GENERATOR VOLTAGE IS ABOVE THE THRESHOLD AND THEREFORE THE SWITCH IS OPERATING IN THE OPEN STATE.

In both cases, the voltage jump occurs in much less than 2 ms (the sample rate of the electrometer) and is modeled as a step input.

Both cases produced a voltage that was large enough to open the switch. This is a result of the generator size, which has approximately 20 cm^2 of contact area between triboelectric layers. This means that even a light impact will produce enough voltage to open the switch. To tune the output voltage such that it is closer to the threshold voltage level, a new, smaller generator should be made so that lower level impacts will produce small voltages that will not open the switch.

The voltage from Figures 8 and 9 decayed slowly back to approximately zero over the course of a few minutes. This is because the PDMS layer in the generator is an insulator and becomes charged during the impact. The consequence of this is that the switch will stay in the open position for a few minutes until the voltage decays enough for the beam to pull back into the closed state. In this case the charge decay can be beneficial because it allows the sensor to reset itself after being triggered.

The simplified step voltages are then applied to Equation (8) to see the beam response. The generator output is not applied directly to Equation (8) because the electrostatic force does not scale with the square of the generator voltage. The voltage is approximated as a series of two steps so that the electrostatic force only needs to be simulated at three voltage levels for each plot. If the voltage is assumed to start at 0 V, then only two simulations are necessary to achieve the stepped voltage response. The electrostatic force coefficients in Equation (8)), p_j, become piecewise functions that change suddenly at each jump in Figures 8 and 9. For the dynamic beam analysis, the beam will start at its pulled-in position and experience a jump in voltage at time zero corresponding to the first step in Figures 8 and 9. Then it will receive a second step to the final voltage after a short delay. The beam responses are shown in Figures 10 and 11. In both cases, the beam is released from its initial pulled-in position showing the switch opens from the shock the generator experiences.

For the smaller impact (Figures 8 and 10) the beam first begins to settle around -0.34 μm from the first voltage spike, then jumps up to 0.37 μm after the second spike, which is its final equilibrium position. The larger impact (Figure 11) moves the beam to approximately 2 μm above the substrate from the first spike, and to over 6 μm from the second spike. Because the force is effectively repulsive, there is no voltage limitation on the sensor. This means the sensor should remain mechanically undamaged from a very large voltage spike, which could occur from an unexpectedly large impact.

Because the delay between each voltage step is much longer than the response period, the beam has time to settle to its static position between the two voltage spikes. If the device is operated at very low pressure, this may not be the case. However, for a quality factor of 70, the beam settles to its equilibrium point in about 10 ms, which is roughly the time between voltage steps in Figure 8. If the beam does not have time to settle to its equilibrium position prior to the second spike, the operation of the

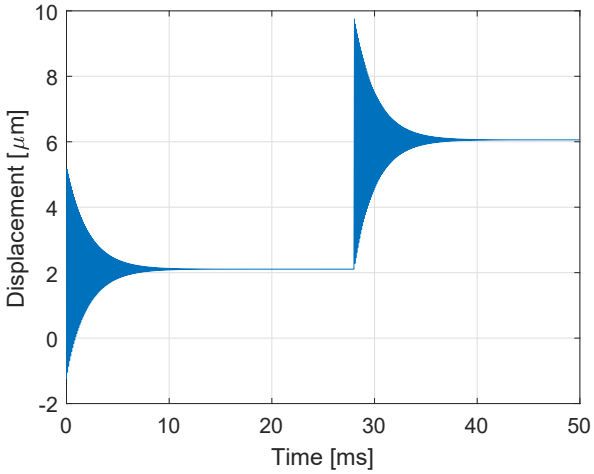

FIGURE 11. BEAM TIP DISPLACEMENT FOR A SIDE VOLTAGE CORRESPONDING TO THE STEP VOLTAGE SHOWN IN FIGURE 9. THE FIRST VOLTAGE STEP IS AT TIME ZERO AND THE SECOND VOLTAGE STEP IS AFTER 28 ms. THE GENERATOR VOLTAGE IS ABOVE THE THRESHOLD AND THEREFORE THE SWITCH IS OPERATING IN THE OPEN STATE.

device should not be affected in most cases.

CONCLUSION AND FUTURE WORK

In this paper a novel shock sensor-switch is presented. The sensor uses a triboelectric generator to convert mechanical energy from an impact to an electrical signal that opens a switch when the impact passes a threshold value. The switch consists of a MEMS cantilever beam with a multi-electrode configuration that can generate both attractive and repulsive forces on the beam. The center electrode is given a small bias voltage to initiate pull-in, and the side electrodes receive voltage from the generator. If the impact is large enough, the repulsive force from the side electrodes releases the beam from pull-in and opens the switch. After a few minutes the charge on the generator decays and the switch resets to its closed state. The theoretical results in this paper have shown that the levitation force is capable of balancing the parallel plate electrostatic force when the beam is in its pulled-in position without tremendously high voltage levels. It has also been experimentally demonstrated that a triboelectric tranducer can generate voltages well above this threshold level and will not immediately discharge when the generator electrodes are left as an open circuit. This design opens the possibility for a new class of electrostatic sensor-switch, which has functionality that would not be possible with traditional electrostatic actuation.

The future work entails fabricating the MEMS switch and a new triboelectric generator, then testing to see if the generator can toggle the switch from closed to open. More in depth analysis of the switch, such as insertion loss, isolation, and reliability, is needed to demonstrate it will work as a switch in practice. Also, ways of reducing power consumption, such as eliminating the need for the 2.2 V bias to create a completely self-powered sensor, will be investigated.

Acknowledgment

This research is funded by NSF grant ECCS #1608692.

REFERENCES

[1] Younis, M. I., 2011. *MEMS Linear and Nonlinear Statics and Dynamics*. Springer, New York.

[2] Miles, R. N., Robert, D., and Hoy, R. R., 1995. "Mechanically coupled ears for directional hearing in the parasitoid fly Ormia ochracea.". *The Journal of the Acoustical Society of America,* ***98***(6), pp. 3059–3070.

[3] Ibrahim, M. I., and Younis, M. I., 2009. "Enhancing the sensitivity of a resonant accelerometer". *2008 Proceedings of the ASME International Mechanical Engineering Congress and Exposition*(11), pp. 241–247.

[4] Miles, R. N., Cui, W., Su, Q. T., and Homentcovschi, D., 2015. "A MEMS low-noise sound pressure gradient microphone with capacitive sensing". *Journal of Microelectromechanical Systems,* ***24***(1), pp. 241–248.

[5] Ramini, A., Younis, M., and Su, Q., 2013. "A low-g electrostatically actuated resonant switch". *Smart Materials and Structures,* ***22***(2), p. 025006 (13 pp.).

[6] Ouakad, H. M., and Younis, M. I., 2013. "Modeling the structural-thermal-electrical coupling in an electrostatically actuated mems switch and its impact on the switch stability". *Mathematical Problems in Engineering,* ***2013***.

[7] Jia, Y., Yan, J., Soga, K., and Seshia, A., 2013. "Parametrically excited MEMS vibration energy harvesters with design approaches to overcome the initiation threshold amplitude". *Journal of Micromechanics and Microengineering,* ***23***(11), p. 114007.

[8] Jia, Y., and Seshia, A. A., 2014. "An auto-parametrically excited vibration energy harvester". *Sensors & Actuators: A. Physical,* ***220***, pp. 69–75.

[9] Park, J. C., Park, J. Y., and Lee, Y. P., 2010. "Modeling and characterization of piezoelectric d33-Mode MEMS energy harvester". *Journal of Microelectromechanical Systems,* ***19***(5), pp. 1215–1222.

[10] Jamain, U. M., Ibrahim, N. H., and Rahim, R. A., 2014. "Performance analysis of zinc oxide piezoelectric MEMS energy harvester". *IEEE International Conference on Semiconductor Electronics, Proceedings, ICSE*(4), pp. 263–266.

[11] Saadon, S., and Wahab, Y., 2015. "From Ambient Vibrations To Green Energy Source : MEMS Piezoelectric Energy Harvester for Low Frequency Application". pp. 59–63.

[12] Huang, F., Fouladi, S., and Mansour, R., 2011. "A novel MEMS-based tunable dielectric resonator filter". *IEEE MTT-S International Microwave Symposium Digest*, pp. 2–5.

[13] Hammad, B. K., Abdel-Rahman, E. M., and Nayfeh, A. H., 2010. "Modeling and analysis of electrostatic MEMS filters". *Nonlinear Dynamics,* ***60***(3), pp. 385–401.

[14] Shen, S., and Young, S., 2002. "Design and fabrication of a MEMS filter bank for hearing aids applications". *2nd Annual International IEEE-EMBS Special Topic Conference on Microtechnologies in Medicine and Biology. Proceedings*, pp. 352–355.

[15] Ahmadi, M., and Jullien, G. A., 2000. "Programmable mems". pp. 522–525.

[16] Bouchaala, A., Jaber, N., Shekhah, O., Chernikova, V., Eddaoudi, M., and Younis, M., 2016. "A smart microelectromechanical sensor and switch triggered by gas". *Applied Physics Letters,* ***109***(1), p. 013502 (4 pp.).

[17] Jaber, N., Ilyas, S., Shekhah, O., Eddaoudi, M., and Younis, M. I., 2018. "Resonant gas sensor and switch operating in air with metal-organic frameworks coating". *Journal of Microelectromechanical Systems*.

[18] Lee, K. B., and Cho, Y. H., 2001. "Laterally driven electrostatic repulsive-force microactuators using asymmetric field distribution". *Journal of Microelectromechanical Systems,* ***10***(1), pp. 128–136.

[19] Sugimoto, T., Nonaka, K., and Horenstein, M. N., 2005. "Bidirectional electrostatic actuator operated with charge control". *Journal of Microelectromechanical Systems,* ***14***(4), pp. 718–724.

[20] Shen, N., and Kan, E., 2002. "Novel electrostatic repulsion forces in MEMS applications by nonvolatile charge injection". *Technical Digest. MEMS 2002 IEEE International Conference. Fifteenth IEEE International Conference on Micro Electro Mechanical Systems (Cat. No.02CH37266)*, pp. 598–601.

[21] He, S., and Ben Mrad, R., 2005. "Large-stroke microelectrostatic actuators for vertical translation of micromirrors used in adaptive optics". *IEEE Transactions on Industrial Electronics,* ***52***(4), pp. 974–983.

[22] He, S., and Ben Mrad, R., 2008. "Design, modeling, and demonstration of a MEMS repulsive-force out-of-plane electrostatic micro actuator". *Journal of Microelectromechanical Systems,* ***17***(3), pp. 532–547.

[23] He, S., and Ben Mrad, R., 2009. "Development of a multilevel repulsive force out-of-plane micro electrostatic actuator". *IECON Proceedings (Industrial Electronics Conference)*, pp. 4020–4023.

[24] Chong, J., He, S., and Ben Mrad, R., 2010. "Control of a surface micromachined repulsive-force driven 2D micromirror". *IEEE/ASME International Conference on Advanced Intelligent Mechatronics, AIM*, pp. 1005–1007.

[25] Fan, C., and He, S., 2015. "A Two-Row Interdigitating-Finger Repulsive-Torque Electrostatic Actuator and Its Application to Micromirror Vector Display". *Journal of Microelectromechanical Systems,* ***24***(6), pp. 2049–2061.

[26] Li, G., Guo, X., Zhao, Q., and Hu, J., 2015. "An Electrostatic Repulsive-Force Based Micro Actuator for Capacitive RF MEMS Switch". pp. 1095–1098.

[27] Qiao, D. Y., Yuan, W. Z., and Li, X. Y., 2006. "Design of an electrostatic repulsive-force based vertical micro actuator". *Proceedings of 1st IEEE International Conference on Nano Micro Engineered and Molecular Systems, 1st IEEE-NEMS*(90407020), pp. 168–171.

[28] Pallay, M., Daeichin, M., and Towfighian, S., 2016. "Dynamic Behavior of an Electrostatic MEMS Resonator with Repulsive Actuation". *Nonlinear Dynamics,* ***89***(2), pp. 1525–1538.

[29] Pallay, M., and Towfighian, S., 2017-67381. "Parametric Excitation of a Repulsive Force Actuator". *Proceedings of the ASME 2017 International Design Engineering Technical Conferences, Aug 6-9, 2017, Cleveland, OH, USA, DETC2017-67381, 7 pages*.

[30] Ozdogan, M., Daeichin, M., Ramini, A., and Towfighian, S., 2017. "Parametric Resonance of a Repulsive Force MEMS Electrostatic Mirror". *Sensors and Actuators A Physical,*. (2017) in press.

[31] Dhakar, L., Tay, F., and Lee, C., 2015. "Broadband vibration energy harvesting using triboelectric mechanism". In International Conference on Experimental Mechanics 2014, International Society for Optics and Photonics, pp. 93021H–93021H.

[32] Du, W., Han, X., Lin, L., Chen, M., Li, X., Pan, C., and Wang, Z. L., 2014. "A three dimensional multi-layered sliding triboelectric nanogenerator". *Advanced Energy Materials,* ***4***(11).

[33] Xie, Y., Wang, S., Niu, S., Lin, L., Jing, Q., Yang, J., Wu, Z., and Wang, Z. L., 2014. "Grating-structured freestanding triboelectric-layer nanogenerator for harvesting mechanical energy at 85% total conversion efficiency". *Advanced Materials,* ***26***(38), pp. 6599–6607.

[34] Zhu, G., Pan, C., Guo, W., Chen, C.-Y., Zhou, Y., Yu, R., and Wang, Z. L., 2012. "Triboelectric-generator-driven pulse electrodeposition for micropatterning". *Nano letters,* ***12***(9), pp. 4960–4965.

[35] Niu, S., Liu, Y., Wang, S., Lin, L., Zhou, Y. S., Hu, Y., and Wang, Z. L., 2013. "Theory of sliding-mode triboelectric nanogenerators". *Advanced Materials,* ***25***(43), pp. 6184–6193.

[36] Zhang, C., Zhou, T., Tang, W., Han, C., Zhang, L., and

Wang, Z. L., 2014. "Rotating-disk-based direct-current triboelectric nanogenerator". *Advanced Energy Materials,* ***4***(9).

[37] Zhu, G., Chen, J., Zhang, T., Jing, Q., and Wang, Z. L., 2014. "Radial-arrayed rotary electrification for high performance triboelectric generator". *Nature communications,* ***5***.

[38] Lin, L., Wang, S., Niu, S., Liu, C., Xie, Y., and Wang, Z. L., 2014. "Noncontact free-rotating disk triboelectric nanogenerator as a sustainable energy harvester and self-powered mechanical sensor". *ACS applied materials & interfaces,* ***6***(4), pp. 3031–3038.

[39] Zhang, H., Yang, Y., Zhong, X., Su, Y., Zhou, Y., Hu, C., and Wang, Z. L., 2013. "Single-electrode-based rotating triboelectric nanogenerator for harvesting energy from tires". *Acs Nano,* ***8***(1), pp. 680–689.

[40] Ibrahim, A., Ramini, A., and Towfighian, S., 2018. "Experimental and theoretical investigation of an impact vibration harvester with triboelectric transduction". *Journal of Sound and Vibration,* ***416***, pp. 111–124.

[41] Rao, S. S., 2010. *Mechanical Vibrations*, Vol. 67. Pearson Prentice Hall.